# Applying the Drive Shaft Torsional Vibration Control to Induction Motors

**Kohei Kawasaki [1] Sho Ohno [1] Hiroyuki Komatsu [1] Yui Ito [1] Akira Sawada [1] Takashi Nakajima [1]**

*1) Nissan Motor Co., Ltd., 560-2 Okatsukoku, Atsugi, Kanagawa 243-0192, Japan,*

*E-mail: k-kawasaki@mail.nissan.co.jp*

**ABSTRACT**: The authors have been developing torsional vibration control for electric vehicles using IPMSM, but it contains rare-earth. While induction motors are one of the rare-earth-less motors, a phase delay of the rotor magnetic flux exists with respect to the stator current. Due to this phase delay, the response of the actual torque to the torque command value exhibits nonlinear characteristics, and a sufficient vibration suppression effect cannot be obtained with the conventional control. In this paper, the authors propose a new torsional vibration control for induction motors and confirm that a smooth acceleration response can be realized through simulations and vehicle experiments.

**KEY WORDS**: EV and HV systems, Motor drive system, Vibration control, Induction motor control

## 1. INTRODUCTION

In recent years, many OEMs have developed electric vehicles (EVs) in response to social demands for environmental protection. Electric motors as power sources are significantly superior to conventional internal combustion engines in terms of torque response, but sudden torque input cause the powertrain system vibrations with a deterioration in ride comfort. We proposed torque vibration control that suppresses the resonance characteristics of the powertrain system to balance the torque response and ride comfort.[(1)-(6)]

On the other hand, induction motors are one of the alternatives which don't use rare earth. However, due to the phase delay between the $\gamma$-axis magnetic flux of the rotor and the stator current, the torque response shows a nonlinear characteristic,[(7)] and because of this characteristic, the conventional vibration control system proposed previously cannot provide sufficient vibration suppression effect. In this paper, we propose a new torque vibration control that considers the phase delay of rotor magnetic flux without sacrificing responsiveness and EV characteristics and show the results of vehicle experiments.

## 2. PROBLEM OF THE CONVENTIONAL CONTROL SYSTEM

### 2.1 Principle of induction motors

The voltage equation on the γ-δ coordinates is expressed as Eq. (1) .

$$\begin{bmatrix} v_{\gamma s} \\ v_{\delta s} \\ 0 \\ 0 \end{bmatrix} = \begin{bmatrix} R_s + sL'_s & -\omega L_s & sM'_L & -\omega M_L \\ \omega L_s & R_s + sL'_s & \omega M_L & sM'_L \\ sM'_L & -\omega_{se} M_L & R_r + sL'_r & -\omega_{se} L_r \\ \omega_{se} M_L & sM'_L & \omega_{se} L_r & R_r + sL'_r \end{bmatrix} \cdot \begin{bmatrix} i_{\gamma s} \\ i_{\delta s} \\ i_{\gamma r} \\ i_{\delta r} \end{bmatrix} \quad (1)$$

The parameters are defined as follows:

$v_{\gamma s}$ : γ-axis stator voltage

$v_{\delta s}$ : δ-axis stator voltage

$i_{\gamma s}$ : γ -axis stator current

$i_{\delta s}$ : δ -axis stator current

$i_{\gamma r}$ : γ -axis rotor current

$i_{\delta r}$ : δ -axis rotor current

$\omega$ : Stator electric angular velocity

$\omega_{re}$ : Rotor electric angular velocity

$R_s$ : Stator winding resistance

$R_r$ : Rotor winding resistance

$L_s$ : Stator static self-inductance

$L'_s$ : Stator dynamic self-inductance

$L_r$ : Rotor static self-inductance

$L'_r$ : Rotor dynamic self-inductance

$M_L$ : Static mutual-inductance

$M'_L$ : Dynamic mutual-inductance

$\omega_{se}$ : Slip angular frequency

The rotor magnetic flux $\phi_{\gamma r}$ and $\phi_{\delta r}$ are defined by Eq. (2).

$$\begin{cases} \phi_{\gamma r} = M_L i_{\gamma s} + L_r i_{\gamma r} \\ \phi_{\delta r} = M_L i_{\delta s} + L_r i_{\delta r} \end{cases} \quad (2)$$

The motor torque equation is as shown in Eq. (3).

$$T_m = p_m \frac{M_L}{L_r}\left(i_{\delta s}\phi_{\gamma r} - i_{\gamma s}\phi_{\delta r}\right) \tag{3}$$

where the $p_m$ is number of poles pairs.

In general, to simplify the torque equation (3), the slip angle frequency $\omega_{se}$ is calculated as follows, on the condition that $\phi_{\gamma r}$ is zero:

$$\omega_{se} = \omega - \omega_{re} = \frac{M_L R_r}{L_r} \cdot \frac{i_{\delta s}}{\phi_{\gamma r}} \tag{4}$$

On the premise that Eq. (4) holds, the $T_m$ and $\phi_{\gamma r}$ are described as Eq. (5) and Eq. (6), respectively.

$$T_m = p_m \frac{M_L}{L_r} i_{\delta s}\phi_{\gamma r} \tag{5}$$

$$\phi_{\gamma r} = \frac{M_L}{\frac{L_r}{R_r}s + 1} i_{\gamma s} \tag{6}$$

Eq. (6) shows that $\phi_{\gamma r}$ has first order LPF characteristic with respect to $i_{\gamma s}$. Fig. 1 shows the stator current, rotor magnetic flux and motor torque response when the step current command is input. The time constant of the reference responses for actual stator currents $i_{\gamma s}$ and $i_{\delta s}$ are designed to be 2 [ms]. The phase delay of $\phi_{\gamma r}$ is determined by the motor parameters, and in this case, it is approximately 40 [ms]. Focusing on actual motor torque, shown in last panel, torque response changes over time. Before the $i_{\gamma s}$ converges to the command value, motor torque changes quickly. However, after this convergence, the response becomes slower due to $\phi_{\gamma r}$. Thus, the torque response of induction motors exhibits nonlinear characteristics.

### 2. 2 Problems with conventional torsional vibration control when applied to induction motors

The system overview is shown in Fig. 2. The motor controller consists of torsional vibration control, current command map, current control, and speed calculation.

The parameters are as follows:

$\theta_{acc}$ : Accelerator pedal angle
$T_e$ : Driver torque command
$T_v$ : Torsional vibration control torque command
$T_m$ : Motor torque
$\theta_m$ : Motor angle
$\omega_m$ : Motor angular velocity
$i^*$ : Current command
$i$ : Actual current
$v^*$ : Voltage command

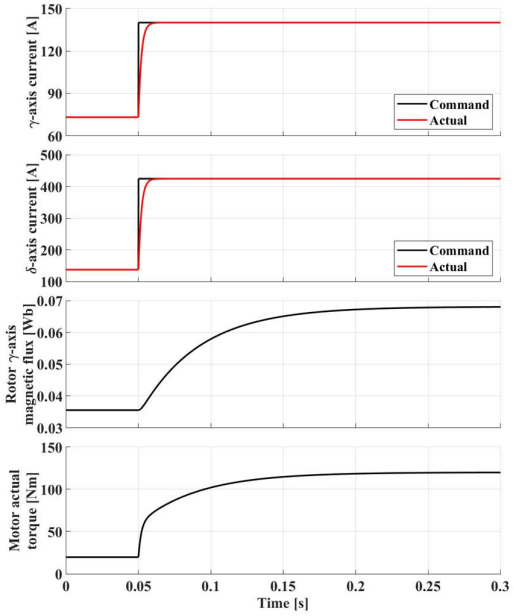


Fig. 1 Simulation results of step current command input

Fig. 3 and Fig. 4 respectively show the models of the drive torque transmission system of an EV and the forward/backward motion of the vehicle body, which were used to derive a system for controlling drive shaft torsional vibration. The equations of motion for the vehicle represented in Fig. 3 and Fig. 4 are expressed as shown below in Eq. (7).

$$\begin{cases} J_m \dfrac{d}{dt}\omega_m = T_m - \dfrac{T_d}{N} \\ 2J_w \dfrac{d}{dt}\omega_w = T_d - rF \\ M\dfrac{d}{dt}V = F \\ T_d = K_d \int \left(\dfrac{\omega_m}{N} - \omega_w\right) dt \\ F = K_t(r\omega_w - V) \end{cases} \tag{7}$$

The parameters are defined as follows:

$J_m$ : Motor inertia
$J_w$ : Drive wheel inertia (One wheel)
$M$ : Vehicle equivalent mass including driven wheel inertia
$K_d$ : Torsional stiffness of the drive shaft
$K_t$ : Coefficient of tire and road surface friction
$N$ : Overall gear ratio
$r$ : Tire Load Radius
$T_m$ : Motor torque
$T_d$ : Drive shaft torque
$F$ : Driving force
$\omega_w$ : Drive wheel angular velocity
$\omega_m$ : Motor angular velocity
$V$ : Vehicle speed

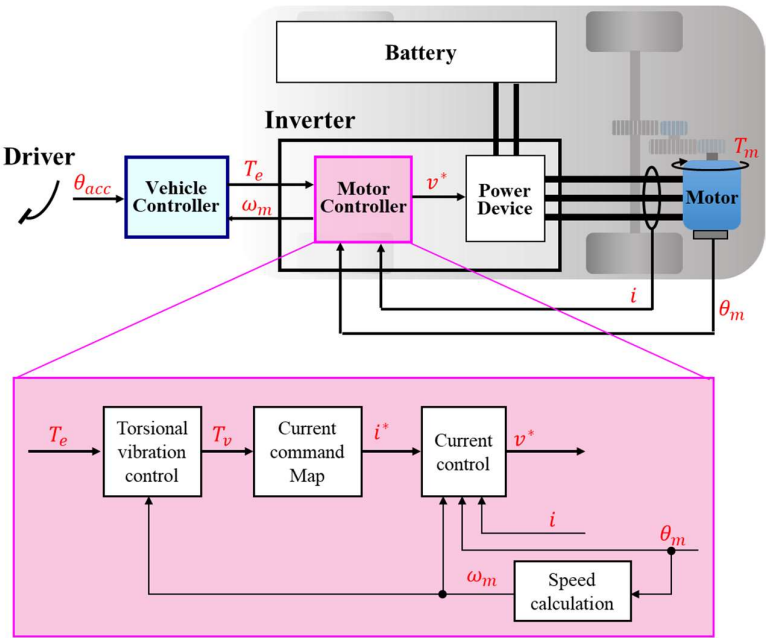


Fig. 2 System overview

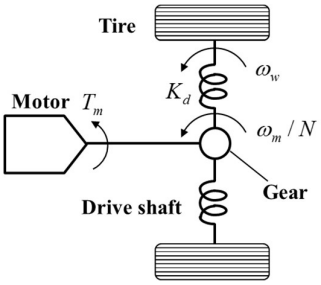


Fig. 3 Driving torque transmission model

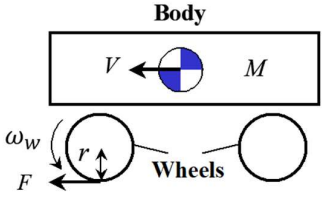


Fig. 4 Model of forward/backward motion of the vehicle body

Based on the equations of motion (7), the transfer characteristics, in which the motor torque $T_m$ is input and the motor angular velocity $\omega_m$ is output, are obtained as in Eq. (8) and Eq. (9).

$$\omega_m = G_p(s)\, T_m \tag{8}$$

$$G_p(s) = \frac{1}{s} \cdot \frac{\beta_3 s^3 + \beta_2 s^2 + \beta_1 s + \beta_0}{\alpha_3 s^3 + \alpha_2 s^2 + \alpha_1 s + \alpha_0} \tag{9}$$

The constants are defined as follows:

$$\alpha_3 = 2J_m J_w M$$
$$\alpha_2 = K_t J_m (2J_w + r^2 M)$$
$$\alpha_1 = K_d M (J_m + 2J_w / N^2)$$
$$\alpha_0 = K_d K_t (J_m + 2J_w / N^2 + r^2 M / N^2)$$
$$\beta_3 = 2J_w M$$
$$\beta_2 = K_t (2J_w + r^2 M)$$
$$\beta_1 = K_d M$$
$$\beta_0 = K_d K_t$$

Eq. (9) is transformed into the Eq. (10).

$$G_p(s) = \frac{1}{s} \cdot \frac{\beta_3 s^3 + \beta_2 s^2 + \beta_1 s + \beta_0}{\alpha_3 (s + a)(s^2 + 2\zeta_p \omega_p s + \omega_p^2)} \tag{10}$$

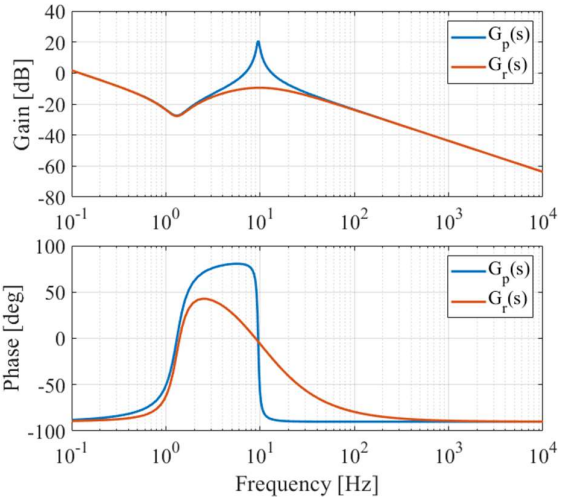


Fig. 5 Frequency characteristics of $G_p(s)$ and $G_r(s)$

The frequency response characteristics of $G_p(s)$ that has a resonance characteristic due to the elasticity of the drive shaft are shown in Fig. 5. The fast rate of change in motor torque causes resonance frequency vibrations in the motor angular velocity, drive shaft torque, and longitudinal acceleration.

The simulation results for the case of a step input of the torque command are presented in Fig. 6. It can be observed that, in the absence of torsional vibration suppression control, fluctuations in the resonant frequency occur in the motor angular velocity, drive shaft torque, and longitudinal acceleration.

Thus, sudden changes in torque can lead to the occurrence of vibrations, resulting in a deterioration of ride comfort. Similarly, torque fluctuations caused by disturbances can also induce such vibrations. Drive shaft torsional vibration control has been devised to eliminate vibrations resulting from sudden torque changes and disturbances. The torsional vibration suppression control transforms $G_p(s)$ into non resonance characteristics $G_r(s)$ shown in Fig. 5.

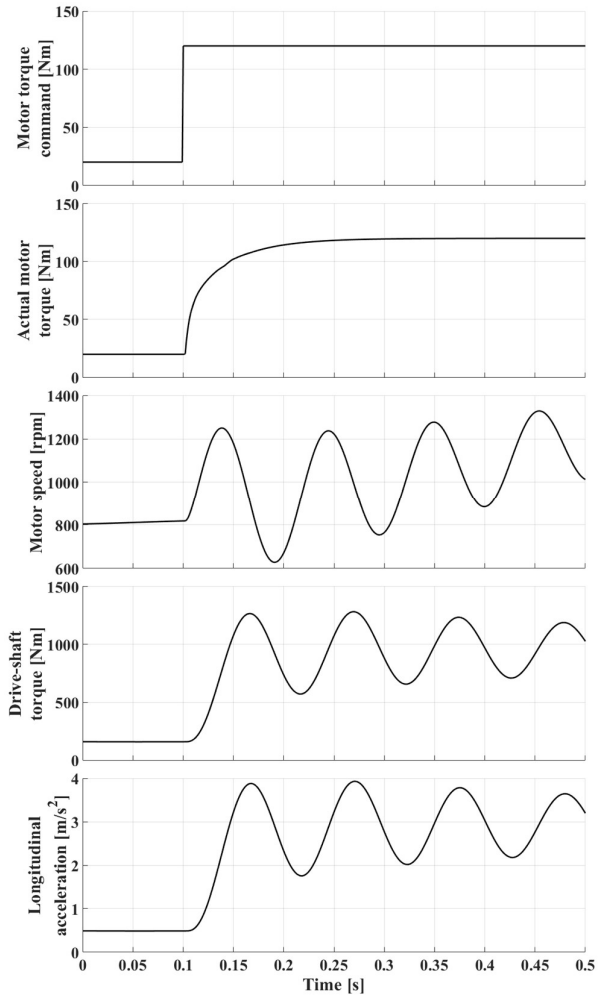


Fig. 6 Torque step input results without control

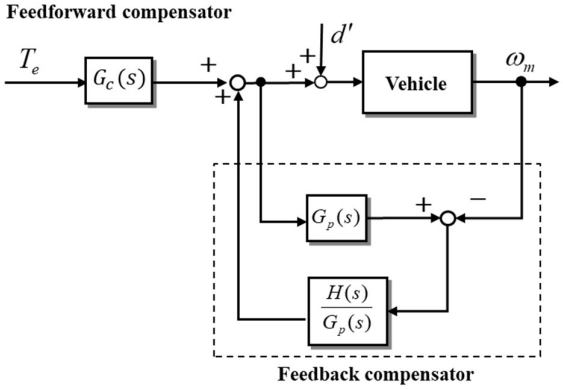


Fig. 7 Torsional vibration control

As shown in Fig. 7, the system for controlling drive shaft torsional vibration consists of a feedforward compensator and a feedback compensator. The feedforward compensator $G_c(s)$ is composed of the desired transfer function $G_r(s)$ and vehicle model $G_p(s)$, as shown in Eq. (11). As a result, when there is no disturbance $d'$, the response of $\omega_m$ to the torque command value $T_e$ can be obtained as shown in Eq. (12).

$$G_c(s) = \frac{G_r(s)}{G_p(s)} \tag{11}$$

$$\omega_m = G_r(s)T_e \tag{12}$$

However, actual vehicles are subjected to various disturbances typified such as sensor error, and modeling error. The feedback compensator, consisting of vehicle model $G_p(s)$ and a bandpass filter $H(s)$, functions to remove the effects of such disturbances. As shown in Eq. (13), $H(s)$ is composed of the natural frequency $\omega_p$ and damping ratio $\zeta_p$ of $G_p(s)$. As a result, the response of $\omega_m$ to disturbance $d'$ does not have any resonance characteristic, as indicated in Eq. (14).

$$H(s) = \frac{2(1-\zeta_p)\omega_p s}{s^2 + 2\omega_p s + \omega_p^2} \tag{13}$$

$$\omega_m = \frac{1}{s} \cdot \frac{\beta_3 s^3 + \beta_2 s^2 + \beta_1 s + \beta_0}{\alpha_3 (s+a)(s^2 + 2\omega_p s + \omega_p^2)} d' \tag{14}$$

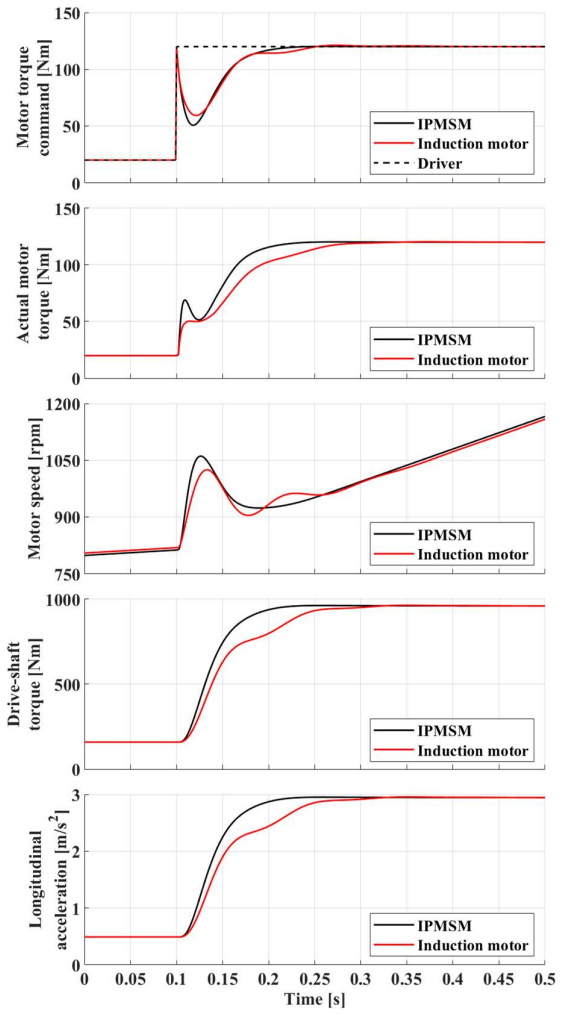


Fig. 8 Simulation results obtained with conventional control

Fig. 8 shows the simulation results of applying conventional control to both the IPMSM and the induction motor with a step driver torque input. In the induction motor, vibrations are observed in both the motor speed and drive-shaft torque. As previously mentioned, induction motors exhibit a phase delay of the rotor magnetic flux with respect to the stator current, resulting in a nonlinear response of the actual torque to the torque command value. Therefore, in conventional control, it is not feasible to consider the plant as a linear system.

## 3. TORSIONAL VIBRATION CONTROL FOR INDUCTION MOTORS

As shown in Eq. (5) and Eq. (6), $\phi_{\gamma r}$ has first order delay with respect to $i_{\gamma s}$, and $T_m$ has a nonlinear characteristic with $T_v$ in induction motors. To suppress the torsional vibration effectively, it is necessary to consider the nonlinearity. However, in the conventional control, the torsional vibration control is applied directly to the torque command without considering the nonlinearity.

Fig. 9 shows the proposed control for induction motors. In this system, only the δ-axis current command value $i_{\delta s}^{*}$ is manipulated. The $\gamma$-axis current command value $i_{\gamma s}^{*}$ is synchronized to driver torque command $T_e$.

First, the current command map determines $i_{\gamma s}^{*}$ and $i_{\delta s}^{**}$ from $T_e$. Then, the flux model calculates the magnetic flux $\phi$ which is defined by Eq. (15).

$$\phi = p_m K_\phi \phi_{\gamma r} \tag{15}$$

$K_\phi$ is defined as Eq. (16).

$$K_\phi = \frac{M_L^2}{L_r} \tag{16}$$

The value of $K_\phi$ changes depending on motor speed and torque. Therefore, $K_\phi$ is calculated by the map to ensure the performance of vibration suppression.

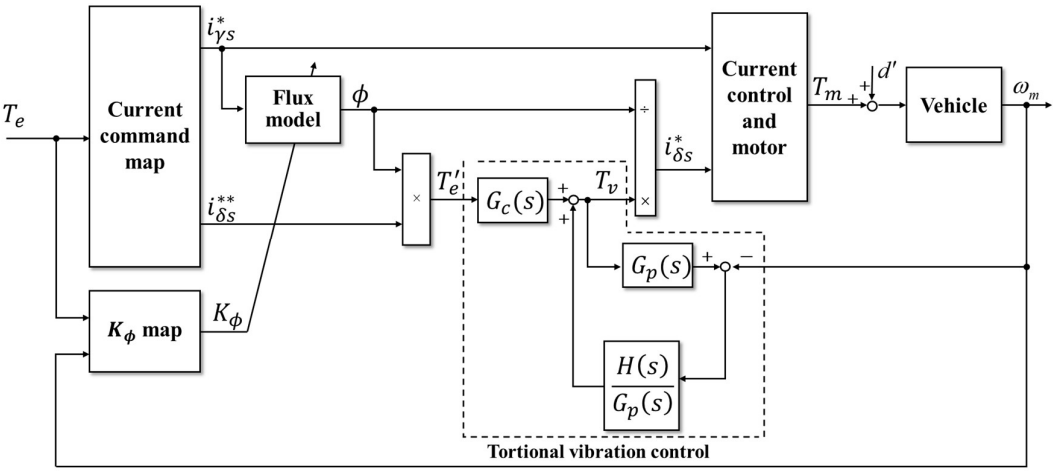


Fig. 9 Torsional vibration control for induction motors

Subsequently, the reference torque $T_e'$ is calculated from $\phi$ and $i_{\delta s}^{**}$. This reference torque $T_e'$ incorporates the specific torque response of induction motors. The torsional vibration control, which remains the same as in the conventional control described in Fig. 4, calculates the $T_v$. Finally, $\delta$-axis current command $i_{\delta s}^{*}$ is recalculated from $T_v$ and $\phi$.

This approach offers two key advantages:

- The nonlinear aspects regarding the torque response of induction motors are excluded, as the feedforward and feedback compensations are performed on the reference torque $T_e'$. Consequently, the torsional vibration suppression performance is not compromised by the torque nonlinearity of induction motors.
- The robustness against disturbances is enhanced, as the feedback compensation utilizes only the δ-axis current, which has a faster response.

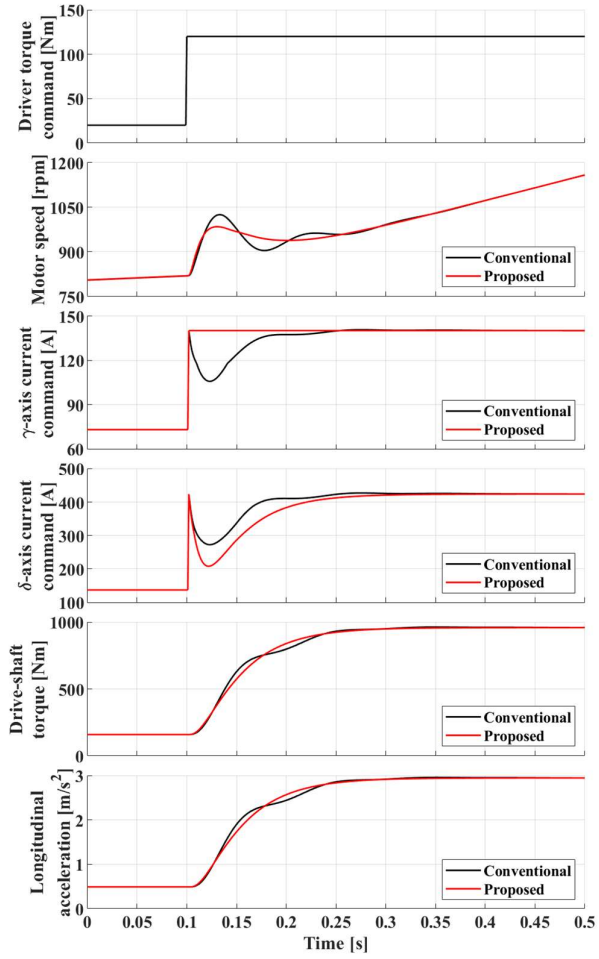


Fig. 10 Simulation results of conventional control and proposed control

## 4. SIMULATION AND VEHICLE EXPERIMENT RESULTS

### 4. 1 Simulation results and the effect of parameter errors

Fig. 10 shows the simulation results of the conventional control and the proposed control where step torque is input.

In conventional control, vibrations occur in the motor's speed and the torque of the drive shaft after a step torque command is input. In the proposed control, vibration is suppressed, and the motor speed and the drive shaft torque change smoothly. Thus, the effectiveness of the proposed control is revealed in the simulation.

As mentioned before, the proposed control is affected by the value of $K_\phi$. In order to mitigate the effects of parameter variations, $K_\phi$ is calculated by a table, with the driver torque command value and motor speed as input parameters. However, the influence of modeling errors, such as temperature dependence and manufacturing uncertainties, cannot be ignored. It is necessary to verify the robustness of the proposed control against variations in $K_\phi$ through simulations.

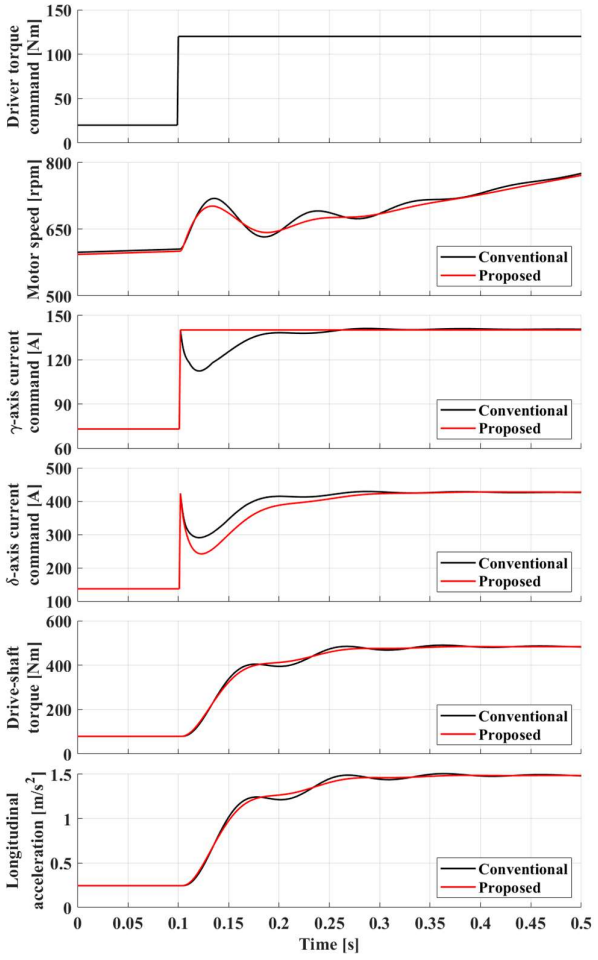


Fig. 11 Simulation results when $K_\phi$ is half of the nominal value

Fig. 11 shows the simulation results when $K_\phi$ is half of the nominal value. Compared to the conventional control, it is obvious that the proposed control can converge the vibrations more quickly. The proposed control improves robustness against disturbances, thereby achieving effective vibration suppression even in the presence of parameter errors.

### 4. 2 Vehicle experimental results

Two types of vehicle experiments were conducted using the Nissan SAKURA, a 2WD kei car, to validate the effectiveness of the proposed control:

- Torque step input from 20 [Nm] to 120 [Nm]
- Torque step input from -10 [Nm] to 90 [Nm]

Fig. 12 shows the vehicle experiment results with the step torque from 20 [Nm] to 120 [Nm]. While the conventional control causes slight vibration in motor speed and drive shaft torque, the proposed control can smoothly converge the vibration. These experiment results exhibit a trend that is consistent with the simulations. Fig. 13 shows the experimental results with a step torque from $-10$ [Nm] to 90 [Nm]. In this condition, the difference in control performance becomes more noticeable due to the backlash in the gears. In the conventional control, it can be observed that, larger vibrations occur in the motor speed, drive shaft torque and longitudinal acceleration. However, in the proposed control, vibrations can be suppressed, that allows a smooth shift from deceleration to acceleration. Through these two types of experiments, the effectiveness of the proposed control has been validated.

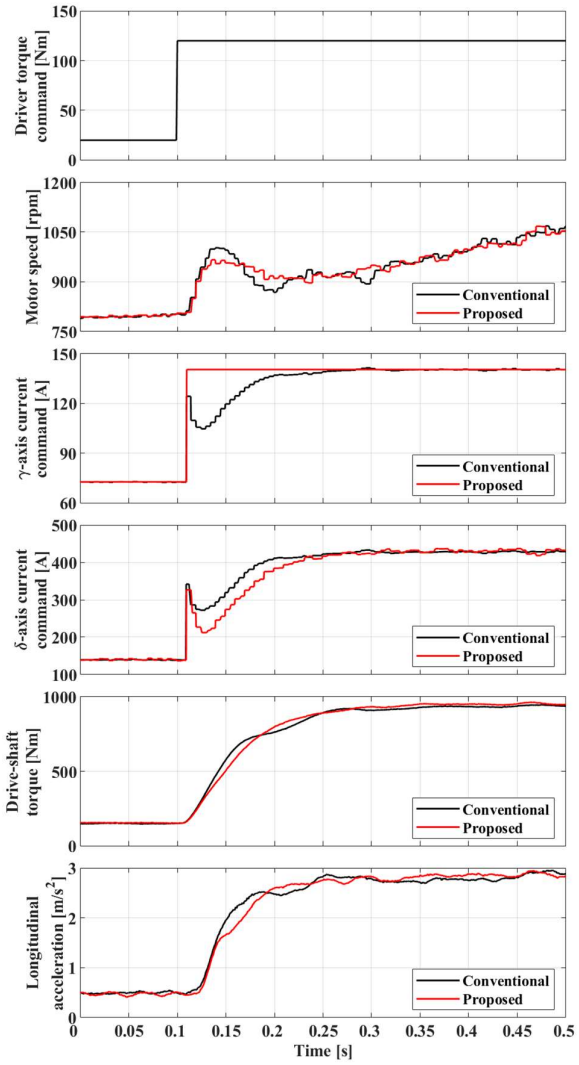


Fig. 12 Vehicle experimental results (from 20 [Nm] to 120 [Nm])

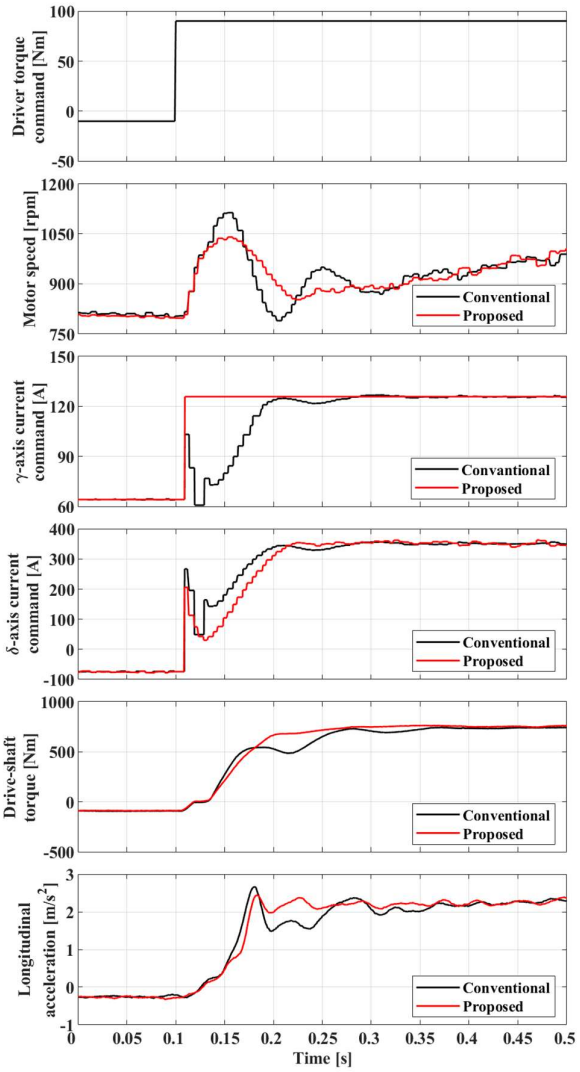


Fig. 13 Vehicle experimental results (from -10 [Nm] to 90 [Nm])

## 5. CONCLUSIONS

While induction motors are one of the rare-earth-less motors, torque response has nonlinearity because of the phase delay of the rotor magnetic flux with respect to stator current. This nonlinearity results in insufficient vibration suppression effects.

In this paper, the authors proposed a new torsional vibration control for induction motors. In the proposed control, the torsional vibration suppression performance is not compromised by the torque nonlinearity of induction motors.

We confirmed the effectiveness of the proposed control through simulations and vehicle experiments.

## REFERENCES

(1) Hiromichi Kawamura, et al, Highly-Responsive Acceleration Control for the Nissan LEAF Electric Vehicle, SAE Paper No.2011-01-0397, (2011).

(2) Sho Ohno, et al, Drive Motor Control Method for Suppressing Drive Shaft Torsional Vibration due to Gear Backlash. Nissan Technical Review 2018(82):23–30, (2018).

(3) Sho Ohno, et al, EV Drive Motor Control for e-Pedal Driving, JSAE Congress (Autumn), 275 (2017).

(4) K.Yoshimoto, T.Hanyu, NISSAN e-POWER: 100% Electric Drive and Its Powertrain Control, IEEJ Journal of Industry Applications,10–4,411/416 (2021)

(5) A.Sawada, et al, A Vertical vibration reduction by new electric motor control in dry sand condition, EVS36 Paper (2023).

(6) Kazunari Moriya, et al, Design of the Surge Control Method for the Electric Vehicle Powertrain, SAE Technical Paper 2002-01-1935, (2002).

(7) Shinji Shinnaka, A Unified Vector Analysis for Vector Control of Induction Motors, Trans. Soc. Instrum. Contr. Eng., vol. 30, no. 7, pp. 760-766, (1994).